Sensors **2006**, *6*, 193-207

sensors

ISSN 1424-8220

http://www.mdpi.org/sensors

Special Issue on "Satellite Altimetry: New Sensors and New Application" Edited by Ge Chen and Graham D. Quartly

Full Research Article

Combined Wind Vector and Sea State Impact on Ocean Nadir-Viewing Ku- and C-Band Radar Cross-Sections

Ngan Tran [1,*] and Bertrand Chapron [2]

[1] Direction Océanographique Spatiale, Collecte Localisation Satellites, 8-10 Rue Hermès, 31520 Ramonville St-Agne, France

[2] Centre ERS d'Archivage et de Traitement, Institut Français de Recherche pour l'Exploitation de la MER/Centre de Brest, B.P. 70, 29280 Plouzané, France

E-mail: Bertrand.Chapron@ifremer.fr

* Author to whom correspondence should be addressed. E-mail: ntran@cls.fr

Received: 26 July 2005 / Accepted: 19 November 2005 / Published: 8 March 2006

Abstract: The authors report the first results in studying the polarization anisotropy of the microwave backscatter from nadir observations provided by Jason-1 altimeter in both Ku- and C-band. A small but clear wind direction signal for wind speeds above 6 m/s is revealed. These azimuthal variations of radar cross-section increase with increasing wind speed up to 14 m/s. The signatures then level off at higher winds. These results extend, for the first time, recent theoretical improved scattering approximation, and point some similarities between scattering and emission mechanisms at nadir. The observed directional effect can thus be interpreted as a signature of the curvature anisotropy of wind-generated short-scale waves. Sensitivities to both wind speed and sea state are also reported in the present analysis.

Keywords: Altimeter, radar cross section, polarization, wind direction, sea state.

1. Introduction

It is well known that off-nadir microwave radar cross-section and emissivity (through brightness temperature) measurements from the ocean depends on surface roughness strength and direction which in turn depends primarily on local surface wind vector. In particular, distinct signatures with respect to the angle between the wind direction and the instrument look direction are observed under different

geometry configurations by both scatterometers and radiometers to help both wind speed and direction retrieval. To date, five spaceborne scatterometers have been successfully deployed after the instrument SASS on Seasat mission in 1978 to follow this concept to operationally provide global ocean winds. The directional signal in passive microwave data was observed from space by Wentz [1] from the Special Sensor Microwave Image (SSM/I) measurements at 53° of incidence angle. Today, the WindSat instrument is a microwave polarimetric radiometer and also provides wind vector retrievals over the world's oceans. However, while the ability of satellite microwave radiometers to retrieve wind speed is certainly well established, wind direction retrieval is still challenging and usually depends on the wind speed [2]. Interestingly, experimental studies also confirmed the sensitivity of passive microwave measurements on ocean wind direction at nadir incidence [3-6], indicating a direction detection capability for passive spaceborne nadir-looking systems. Combined with theoretical investigations [7-10], these results have suggested that nadir-looking radiometer directional sensitivity follows from the azimuthal anisotropy of the spatial curvature spectrum of short-gravity and capillary waves. Such expected signatures were further documented from TOPEX radiometer data [11]. Intuitively, from reciprocity between emissivity and reflectivity, such a directional sensitivity might also be expected on nadir radar cross section measurements. From a theoretical point of view, recent developments (e.g. review from [12]) highlighted the potential surface curvature correction to the Kirchhoff approximation to also predict a nadir polarization signature related to an azimuthal anisotropy of the surface curvature.

The purpose of the present investigation is to confirm or invalidate this assumption over the ocean surface. The present work is based on the use of data from the Jason-1 altimeter. The analysis has been carried for both Ku- (2.1 cm radiation wavelength) and C-band (5.5 cm). These coincident dual-frequency measurements then further help to discriminate the potential sources of surface anisotropy signatures. Indeed, the differential scattering, Ku- vs. C-band measurements, is mostly governed by the small gravity-capillary roughness elements [13,14]. To the authors' knowledge, this analysis presents the first attempt to evidence a wind direction dependency on radar cross-section at nadir-viewing. For off-nadir geometry, this dependency is based on the azimuth angle between the antenna look direction and the wind direction. At nadir-viewing geometry, the azimuth angle turns into the angle between the polarization plane and surface wind vector. As already demonstrated in previous analysis (e.g. [15, 11, 16]), our methodology is based on a co-location strategy. Here, we took advantage of the availability of an extensive collocation dataset between radar cross-section measurements and independent wind fields from the European Centre for Medium-Range Weather Forecasts (ECMWF) model surface wind analyses. Data are presented in section 2. Sections 3 and 4 report the wind vector analysis and the combined wind vector and sea state (through the altimeter significant wave height parameter) analysis for the two frequency radar cross section measurements, respectively. A final section provides conclusions.

2. Data

On December 7, 2001, the Jason-1 satellite was launched to continue the successful TOPEX/Poseidon (T/P) mission starting in 1992. This new satellite, also jointly developed by the French and U.S. space agencies (CNES/NASA), was placed in the same orbit as T/P (1336 km of

altitude and 66° of inclination) and provides data at a level of performance identical to its predecessor. The Poseidon-2 altimeter aboard Jason-1 uses two channels at 13.6 GHz (Ku-band) and 5.3 GHz (C-band) [17]. The altimeter radar cross-section sample (σ_0) represents an average over an area whose diameter is between 2 and 8 km and is larger when the significant wave height (SWH) in the footprint is large [18], and this is smeared by the 6 km traveled in the nominal 1-s averaging period.

To perform the present analysis, we used a large data set extracted from Geophysical Data Records (GDR) products combining ECMWF wind vector with Jason-1 measurements of σ_0 and SWH over 179 days spanning a 3-year period (from 2002 to 2004). The selected days are characterized by a particular configuration of the satellite on its orbit. Indeed, changes in Jason-1 spacecraft yaw angle are frequent and designed to maintain good exposure of the solar panel to the Sun. There are two modes, a fixed yaw mode (during which spacecraft is commanded to travel in a fixed yaw orientation aligning the vehicle roll axis (+x-body axis) parallel to the velocity vector) and a sinusoidal yaw mode (during which the spacecraft follows a sinusoidal yaw slewing profile when traveling). The selected days are associated with the fixed yaw states (0° or 180° depending on the betaprime angle sign that defines the angle between the orbit plane and the sun-line) that allows simple calculation of a relative azimuth direction, ϕ, that is defined as the ECMWF wind direction minus the Ku-band antenna polarization direction. Note that, from the antenna design, the electric vector $\vec{E}$ of the Ku-band radiation coincides with the spacecraft +x-body axis (flight course of the spacecraft when flying forward) while the vector $\vec{E}$ of the C-band radiation is perpendicular to it (Carayon 2005, personal communication). We will use hereafter the alignments of the Ku-band linear polarization vector as reference to compute the relative wind direction ϕ referred as the wind angle for analyzing the data from both frequencies. So denoting the azimuth angle of the Ku-band polarization direction by ϕ_{Ku} and the wind direction by ϕ_w, both with respect to the North reference, the relative wind direction is defined as: $\phi = \phi_w - \phi_{Ku}$. When ϕ is 0° (180°), the Ku-band polarization is parallel (anti-parallel) to the wind direction. "Crosswind" observations (in which the polarization is orthogonal to the wind direction) occur when ϕ is 90° and 270°. These configurations are reversed for the C-band (C-band polarization is parallel to the wind direction when ϕ is 90°).

3. Wind vector impact

3.1. Modeling

Figure 1 shows the Ku-band radar cross-section averaged within 10° bins as a function of the azimuth angle ϕ for different wind speeds at ± 0.5 m/s. A 3σ filter was applied within each bin to eliminate outlier measurements. The statistical indicators computed within each bin (mean and standard deviation) are plotted only when at least 500 measurement samples were used to determine them. As found, there are clear azimuth modulations even at a low wind speed of 3 m/s. These features are also observed for C-band data as illustrated in Figure 2.

In view of the behaviour displayed in Figure 1, the relative wind direction dependence was first empirically modelled by general second-order Fourier series. Commonly, the azimuthal dependence on radiometer and scatterometer data is assumed to be well represented by second-order cosine expansion regression with maxima occurring at 0 and 180° and minima at 90°. However, the present

observational investigation is not as clear regarding this assumption. An offset angle is thus introduced, to model the nadir cross section measurements as:

$$\sigma_0 = a0 + a1 \cos(\phi - \phi_1) + a2 \cos 2(\phi - \phi_1) \quad (1)$$

Evaluation of a1 from least-square regressions generally shows these coefficients of the order of 10 times lower than a2. The model has thus been simplified as:

$$\sigma_0 = a0 + a2 \cos 2(\phi - \phi_1) \quad (2)$$

In this model, the mean backscatter term a0 mainly carries the information on wind speed while a2 accounts for the difference in backscatter extremes and so carries the dependence of the nadir radar cross-section on the azimuth angle. Empirical curves from least-squares fits of the form (2) are provided for each wind speed in Figure 1.

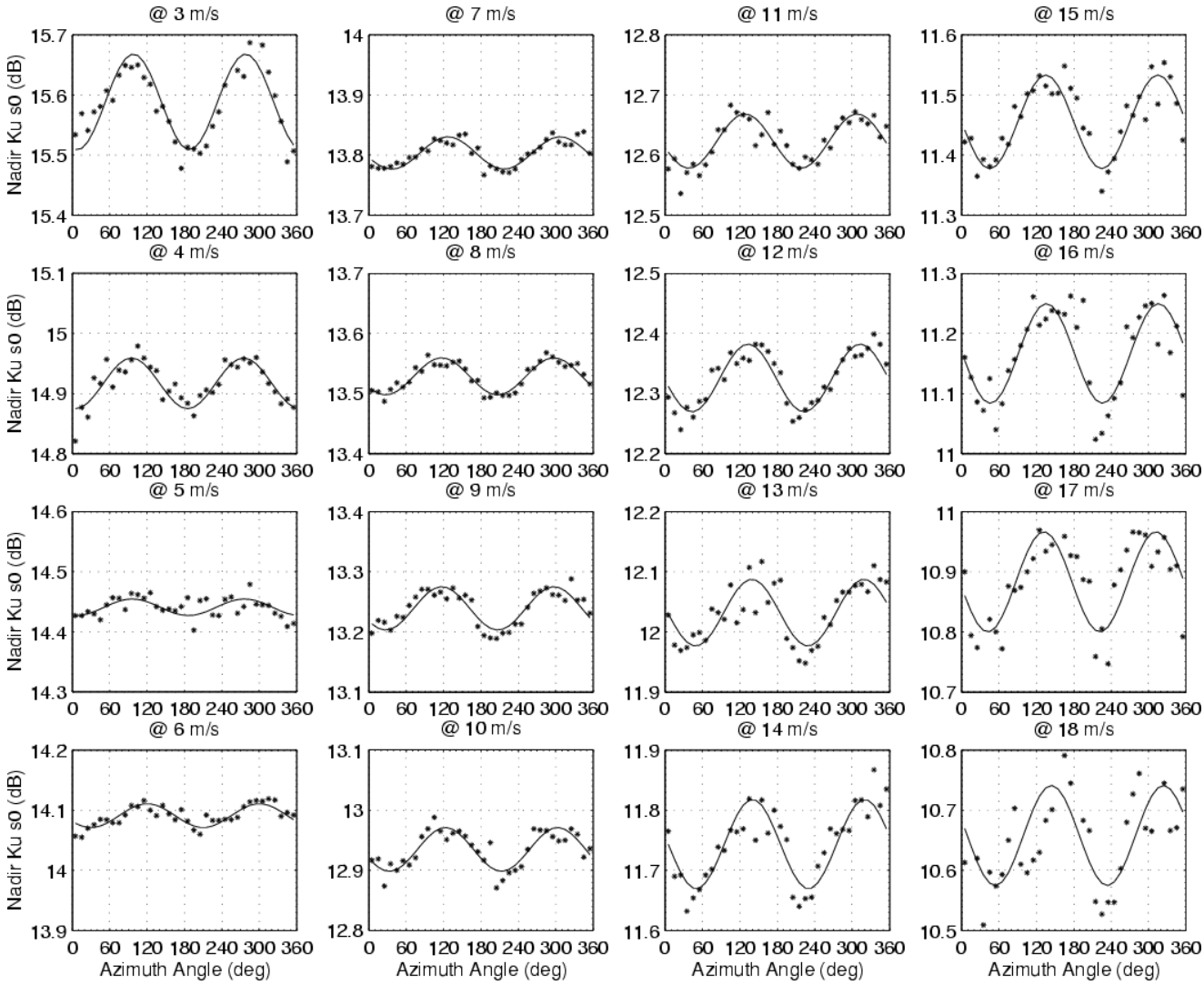

Figure 1. Wind direction signal in 10° bins of the Ku-band altimeter radar cross-section for different wind speeds at ± 0.5 m/s and varying from 3 to 18 m/s. The solid line represents the second-order harmonic fit of form (3).

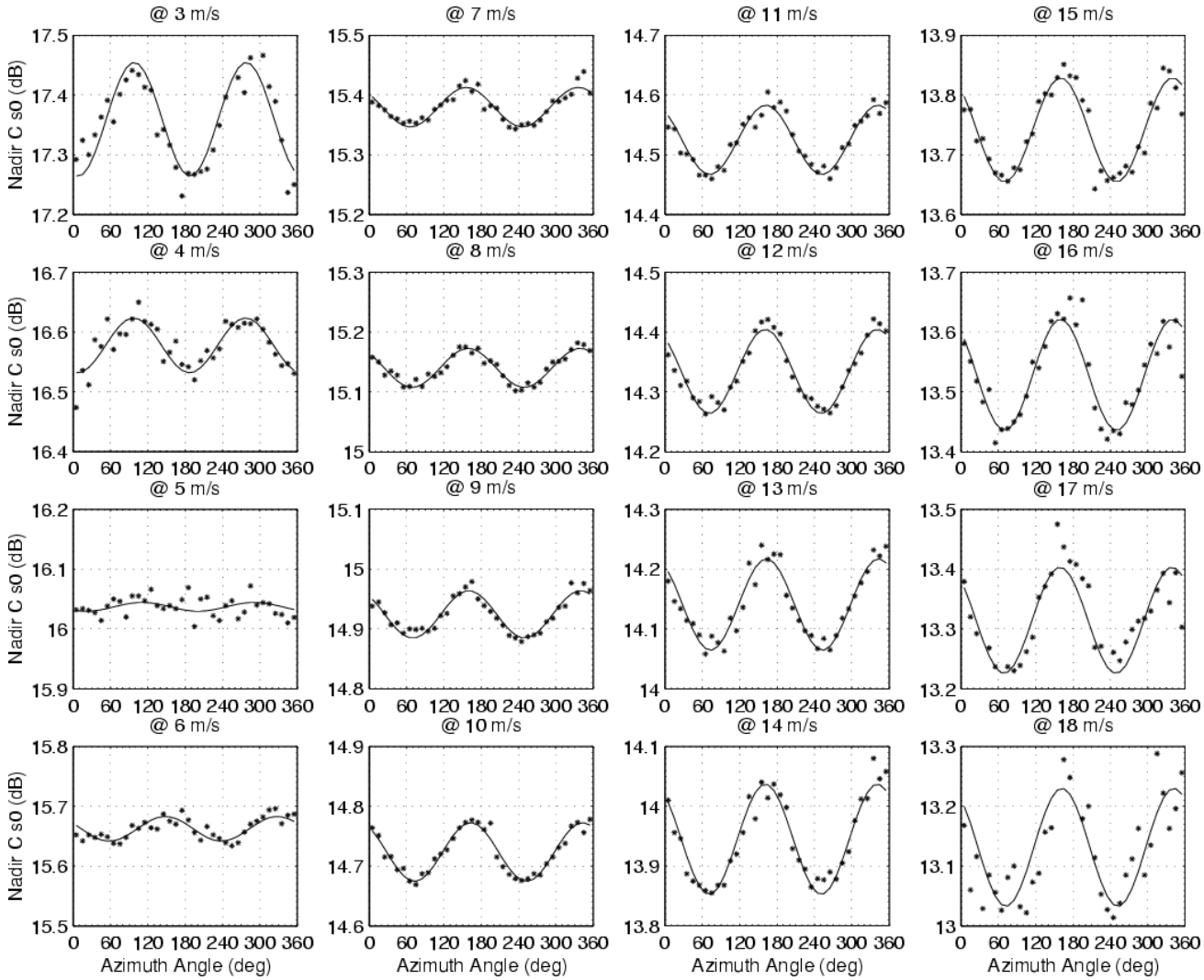

Figure 2. Same as Figure 1 for C-band altimeter radar cross-section.

Although this directional signal is rather small, the peak-to-peak directional signal is lower than 0.1 dB, it is statistically significant, and certainly benefits from the large number of measurements used to reduce the noise in each selected bin. According to these observations, altimeter active microwave measurements are thus also sensitive to the directional property of the surface waves for wind speeds above 5 m/s. Lower wind cases will be discussed separately in the following. These results are somehow consistent with the variations observed on nadir brightness temperatures from TOPEX/Poseidon microwave radiometer at 18, 21, and 37 GHz [11]. The amplitude of the peak-to-peak brightness temperature variation was evaluated to be about 0.8-1.1 K for 18-37 GHz at 11.5 m/s.

3.2. Directional anisotropy strength δ

The feature of the azimuth anisotropy (a2) depends on wind speed. In the wind speed range 6-18 m/s for instance, as the wind speed increases, the average value of the backscatter cross-section decreases and the anisotropy increases. To directly compare Ku- and C-band peak-to-peak azimuthal strength, we present results for a normalized parameter, a depth of azimuthal modulation δ, defined as [19]:

$$\delta = \frac{a0 + a2}{a0 - a2} - 1 \tag{3}$$

Figure 3 gives δ as function of wind speed for both frequencies. As obtained, results are comparable in shape and also in magnitude. There is a clear change in behaviour of the peak-to-peak directional

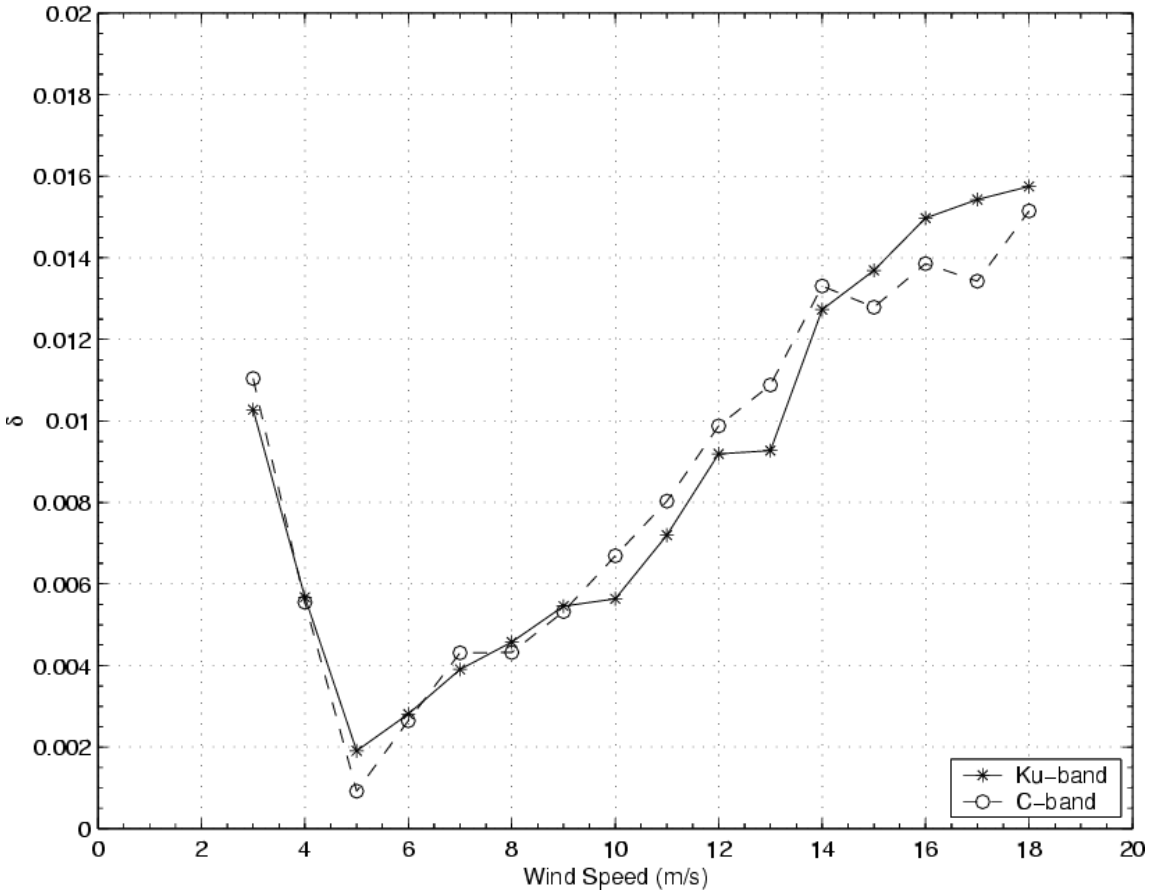

Figure 3. Depth of azimuthal modulation δ at Ku- and C-band as a function of wind speed.

signal at a critical wind speed of about 5 m/s. The magnitude of δ apparently decreases sharply with increasing wind speed in the range 3 to 5 m/s. Then it increases for moderate wind speeds and saturation seems to occur for wind speeds above approximately 14 m/s. The rate of variation with wind speed is nearly the same for the C-band and for the Ku-band data. This behaviour is in some characteristics consistent with the cross section differences between the two frequencies [14] to indicate the governing influence of the short gravity-capillary wind roughness scales. At high wind speed, the apparent saturation may also be compared to C-band scatterometer results [19]. For these higher wind conditions, breaking waves occur with foam and spray potentially leading to a weaker azimuth modulation of short scale roughness elements. At intermediate wind conditions (between 5 and 12 m/s), the cross section anisotropy apparently follows nadir ocean emissivity observations [11]. Note also that there are differences in footprint diameter size between instruments. The footprint is about 20-40 km depending on the microwave frequency for nadir TOPEX/Poseidon radiometer

compared to the smaller footprint of Jason-1 altimeter. The latter is only a few km with an elliptical form for small SWH and a more circular shape at large SWH. This should be kept in mind when comparing sensitivity. This sea state footprint dependency might partially explain the different features observed at 3-5 m/s wind between cross section measurements and emissivity ones at nadir-viewing.

3.3. Direction of σ_0 -maximum indicated by ϕ_1

The second characteristic of the cross section behaviour lies on the position of the maximum values. Traditional observations in scatterometry show that these maximum values coincide with the radar beam directed parallel to the upwind/downwind (U/D) directions. The minimum values then correspond with the radar beam crossing the wind direction for both co-polarization backscattering cross-sections (σ_0^{VV} and σ_0^{HH}). Such signatures of the microwave backscattering from the sea surface are explained by the anisotropic growth of short surface waves (e.g. [20]). In the present data analysis, there is an apparent shift in azimuth position. The maximum values are not always aligned with the U/D directions. This is found for both Ku- and C-band measurements. As shown in Figure 4, ϕ_1 values

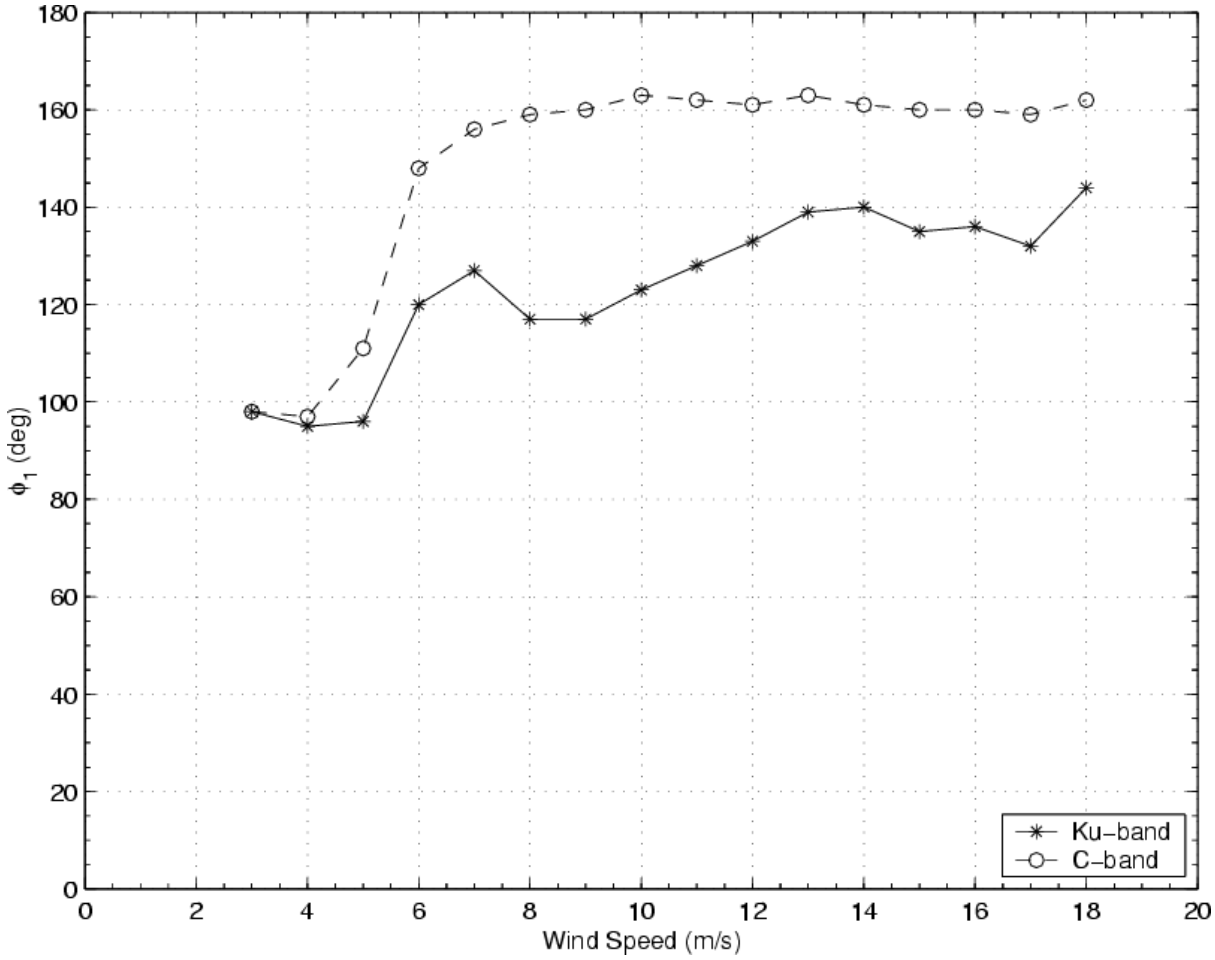

Figure 4. Variation of azimuth angle shift ϕ_1, corresponding to the direction of maximum backscatter signal, as a function of wind speed.

are similar for both frequencies at low wind speeds with values ~90-100° and they are different above 5 m/s wind speed conditions. The C-band values are set at about 160° for wind speeds above 8 m/s. The Ku-band values varies between about 120 to 140° with a slight increase as wind speed increases above 6 m/s. Note that the data processing is identical for the two frequencies and is performed simultaneously such that the frequency-dependent statistical mean within each bin is based on the same mixture of sea surface conditions encountered in the large database. Note also that the variations from the two frequencies are not generally in phase opposition whereas the two vectors $\vec{E}$ (polarization characteristics of the antennas) associated to each frequency are perpendicular to each other.

3.4. Low wind conditions

Results presented above show that for wind speed lower than 6 m/s, the directional anisotropy in the radar cross-section is not antenna polarization orientation dependent. Indeed, as shown in Figure 4, the direction of the maximum of backscatter signal is the same for the Ku- and C-band, while their respective polarization directions are perpendicular. Moreover the maximum corresponds to a fixed 90° orientation from the wind direction. Such a result would suggest that the expected theoretical polarization signature with wind direction does not occur under relatively smooth surface. Indeed, any improvement of the tangent plane approximation shall come through surface slope quadratic and higher order slope derivatives. Under low wind conditions, the sea surface slope variances are small with little to no impact on a polarization signature. Yet, the sea surface slope anisotropy certainly combines with the footprint characteristics to give radar cross section modulation solely in power. Such a result would somehow follow the suggested altimeter technical improvement to estimate wind direction using an asymmetric antenna beam [21]. As found, it thus appears that the antenna correction may not be perfect with the observed (weak) residual wind direction signatures.

3.5. Moderate winds

In the wind speed range 5 - 14 m/s, the relative strength of the azimuthal modulations increases as the wind speed increases. As revealed in Figure 4, the directional contrasts are statistically nearly equal for the two frequencies. But, contrary to the low wind cases, the maximum values do not occur at the same angles for Ku- and C-band measurements. According to the instrument configuration, these directional signatures are thus polarization dependent. Following theoretical developments [22, 12], such a nadir polarization signature shall reflect the fact that the scattering surface can not be considered locally flat, but has finite directional local radii of curvature to modulate the polarization signature. Ultimately, and according to the instrument polarization, the expected directional curvature polarization signature for Ku- and C-band should lead to maximum values in quadrature. The observations do not fully confirm such a theoretical prediction. Yet, as obtained, the C-band measurements somehow better confirm these expected tendencies. Horizontally polarized backscatter signals would indeed be slightly higher at nadir geometry than vertically polarized ones. The fact that Ku-band observations are not found systematically smaller along the wind directions may indicate that the polarisation sensitivity is weaker than at C-band, i.e. the curvature correction to Kirchhoff

scattering solution is frequency dependent. Geometrically, the shorter ripples integrated in a Ku-band measurements compared to C-band ones are indeed expected to modify both the number of specular zero slopes and the mean radius of curvature [23]. Furthermore, the complex interplay between short and large ocean surface roughness scales must also be considered to interpret the results. As known, oblique-angle larger waves can hydro-dynamically modify the shorter scale directional anisotropy [24]. These latter can, in turn, further contribute to modify the surface drag coefficient that result in stress vector shifts towards the long wave directions. The proposed statistical analysis cannot help to distinguish these potential effects, and the brute force binning methodology certainly contributes to blur the exact small scale anisotropy signatures at nadir.

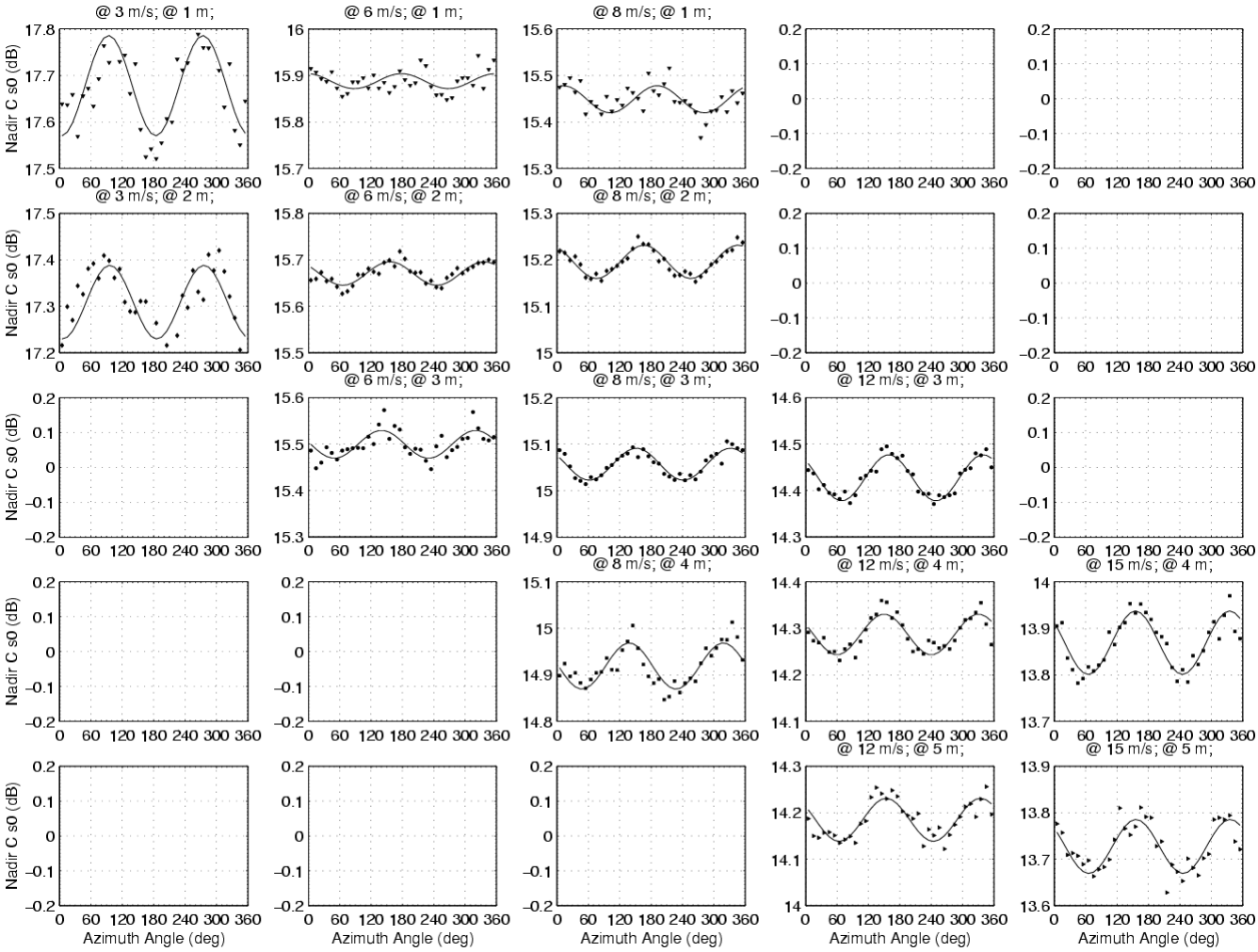

Figure 5. Variation of C-band altimeter radar cross-section with the relative azimuth angle for five different wind speeds from low to high wind forces and different classes of SWH of 1 m interval.

4. Combined impact of wind vector and sea state

In this section, we examine the behaviour of Ku- and C-band cross section measurements according to the sea state altimeter derived parameter SWH, wind speed, and wind angle. The a0, a2, and shift angle coefficients have been estimated as a function of both SWH and wind speed in 1 m and 1 m/s bins, respectively. Figure 5 gives examples of the periodic signatures for C-band measurements for 5 different wind speeds from low to high wind forces and combined 5 SWH classes of 1 m. The addition of the SWH parameter in the analysis seeks to better picture certain combinations of wind and sea state conditions. At 1 m SWH, results can be analysed only in term of low winds (<5 m/s). At higher winds, the sampling population is too poor and the binning results too noisy. Discrimination of data in term of SWH conditions at a given wind speed is found to be only possible for moderate to high wind speeds, between 6 and 14 m/s.

4.1. Analysis of δ

The dependencies of δ as a function of wind speed, SWH, and frequency are provided in Figure 6. As the wind increases above 5 m/s, the depth of modulation slightly increases at both frequencies. However, while the magnitudes of the measured cross section directional anisotropy are nearly SWH independent for the C-band measurements at a given wind speed, there are well-marked SWH impacts on the Ku-band measurements. As statistically revealed, the Ku-band anisotropy increases with SWH. Differences are quite significant. As found, the depth of modulation largely doubles from 0.004 to 0.01 between 2 m and 4 m SWH, respectively, for the 10 m/s wind speed bin. The fact that C-band sensitivity is much weaker to SWH changes may be related to the sea state impact on the very short scale roughness modulation. As generally found [15], the cross section relative differences between C- and Ku-band frequencies are SWH independent under moderate to high wind speed conditions. Accordingly, the shortest roughness scale changes with sea state are then mostly marked in terms of anisotropy modulations rather than energy level variations. Further investigations are certainly needed to interpret these findings and are presently out of the scope of this preliminary statistical analysis.

4.2. Analysis of ϕ_1

Analysis of ϕ_1 estimates displayed in Figure 7 shows distinct dependencies of SWH. For the Ku-band measurements, the SWH filtering helps to refine earlier conclusions. Indeed, the Ku-band cross section maximum values peak now more systematically at an angle that is nearly independent of the wind speed and the sea state conditions. Moreover, this angle is closer to the crosswind direction. As mentioned above, such results are more in line with theoretical developments. As found, at 9 m/s for instance, the maximum value at Ku-band is found at about 115°. At C-band, the maximum values are found to peak near the wind direction. However, there is an apparent SWH impact. As found, a SWH increase tends to lower the polarization signature.

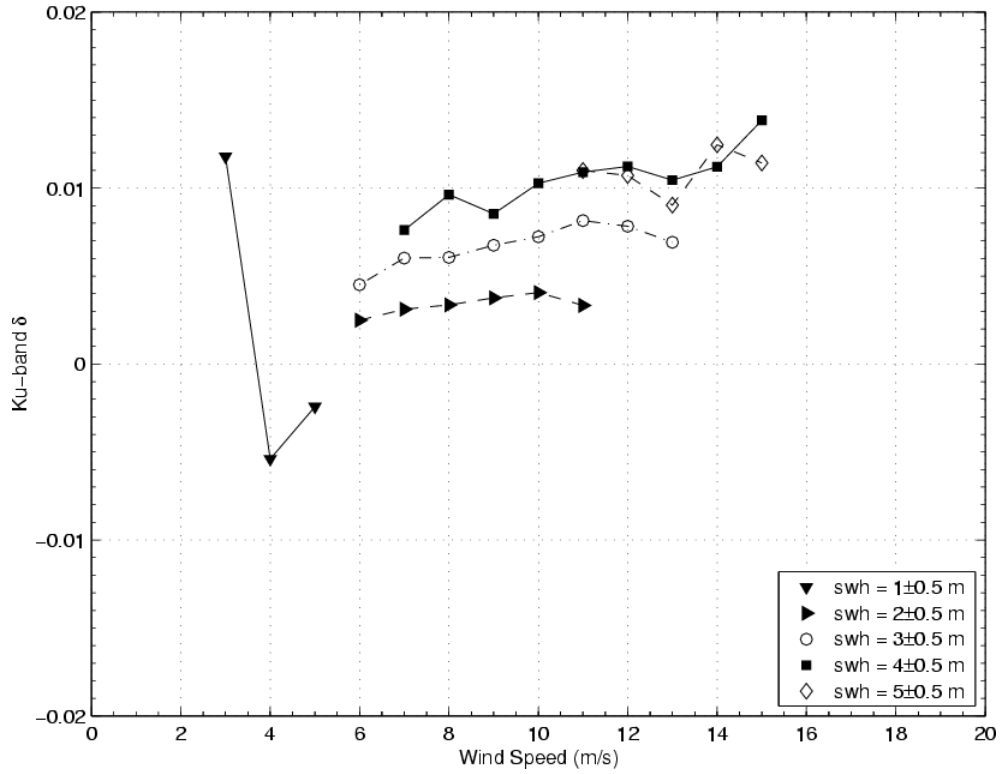

(a)

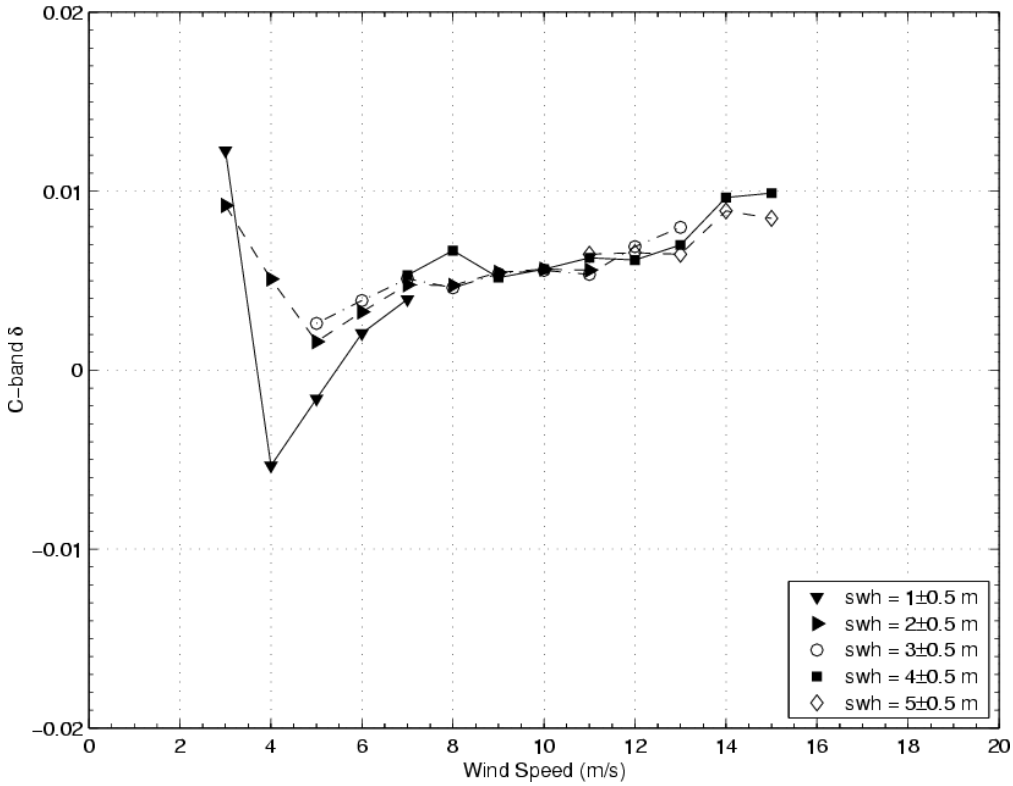

(b)

Figure 6. Same as Figure 3 for five different 1 m SWH classes (a) for Ku-band data and (b) for C-band data.

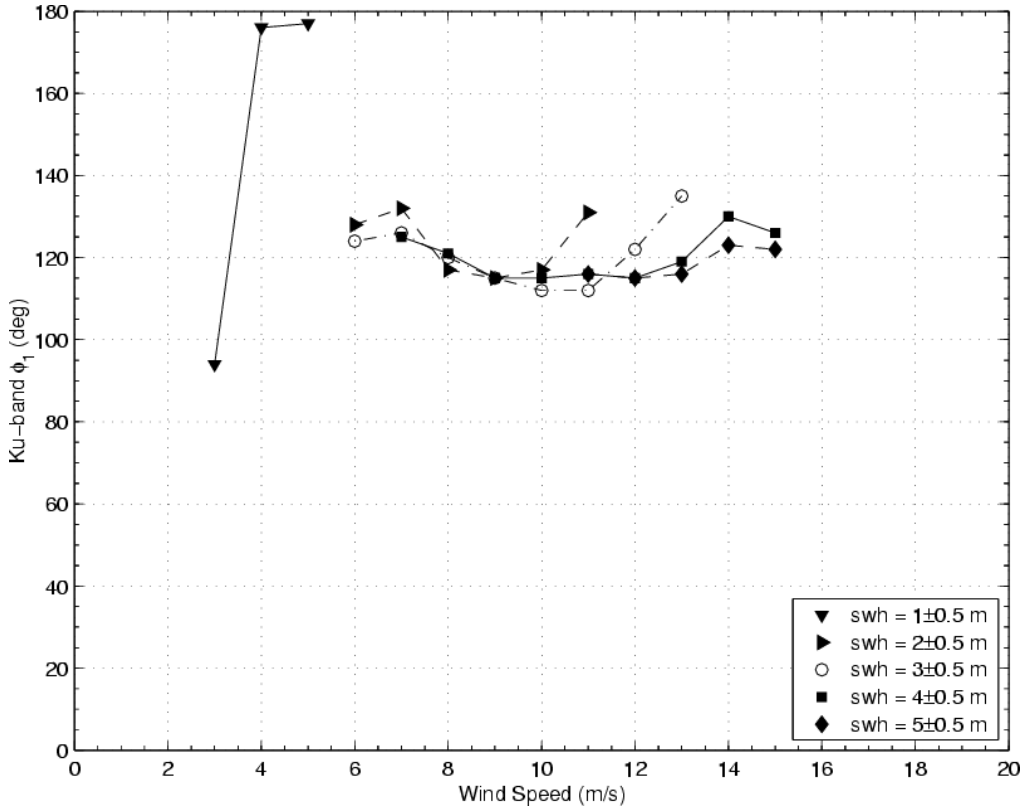

(a)

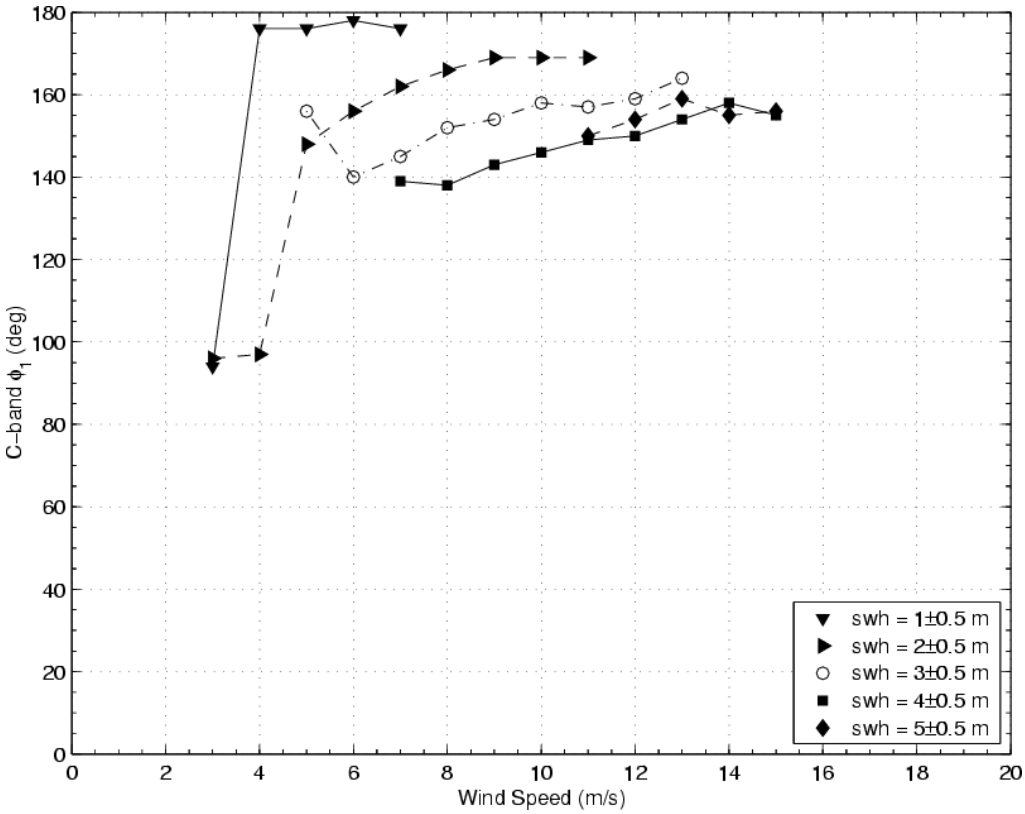

(b)

Figure 7. Same as Figure 4 for five different 1 m SWH classes (a) for Ku-band data and (b) for C-band data.

5. Conclusions

The present results clearly demonstrate, for the first time, the presence of a wind direction signal through the polarization anisotropy in altimeter radar cross-section in both Ku- and C-band measurements. Due to similarities with results from nadir-viewing passive microwave measurements and off-nadir radar cross section ones, these features suggest that the altimeter directional sensitivity also follows from the azimuthal anisotropy of the curvature spectrum of short-gravity and capillary waves under moderate wind speed conditions. The overall magnitude of the directional modulation was found to be frequency independent. Additional conditionality with the inclusion of information on sea state by using altimeter derived SWH parameter has pointed out that this conclusion certainly needs to be qualified. The data used to conduct our investigation were randomly collected over the globe, but it is impossible to provide within this dataset more information on the mutual vector alignments between the emitted radiation and both the wind and large waves directions. The results represent ensemble averages over varied long wave directions of propagation that may not be really uniformly distributed, according to the swell and wind particular distributions over the oceans. It can solely be concluded that the SWH impact on the backscatter anisotropy is not as strong as its effects on the mean backscatter power. This indicates that both the power modulation and the polarization signature are mostly supported by intermediate to short surface scales that contribute the most to specular point and curvature radius modulation. All these new results highlight the sea surface dependency of the scattering mechanism at nadir. Further investigations are certainly needed to better decipher the implications and the potential to consider both frequency and polarization measurements on future altimeter instruments.

Acknowledgements

Thanks are given to G. Carayon for providing information on the polarization state of the altimeter.

References and Notes

1. Wentz, F. J. Measurement of oceanic wind vector using satellite microwave radiometers. *IEEE Trans. Geosci. Remote Sensing* **1992**, *30*, 960-972.
2. Meissner, T.; Wentz, F. J. An updated analysis of the ocean surface wind direction signal in passive microwave brightness temperatures, *IEEE Trans. Geosci. Remote Sensing* **2002**, *40*, 1230-1240.
3. Bespalova, E.A.; Veselov, V. M.; Gershenzon, V. E.; Militskii, Y. A.; Mirovskii, V. G.; Pokrovskaya, I. V.; Rayev, M. D.; Semin, A. G.; Smirnov, N. K.; Skachkov, V. A.; Trokhimovski, Yu. G.; Khapin, Yu. B.; Chistyakov, V. N.; Sharkov, E. A.; Etkin, V. S. Surface wind velocity determination from measurements of the polarization anisotropy of microwave emission and backscatter. *Sov. J. Remote Sensing* **1982**, *1*, 121-131.
4. Trokhimovski, Y.G.; Bolotnikova, G. A.; Etkin, V. S.; Grechko, S. I; Kuzmin, A. V. The dependence of S-band sea surface brightness and temperature on wind vector at normal incidence, *IEEE Trans. Geosci. Remote Sensing* **1995**, *33*, 1085-1088.

5. Kuzmin, A.V.; Pospelov, M. N. Measurements of sea surface temperature and wind vector by nadir airborne microwave instruments in Joint United States/Russia Internal Waves Remote Sensing Experiment JUSREX'92. *IEEE Trans. Geosci. Remote Sensing* **1999**, *37*, 1907-1915.
6. Irisov, V.G. Azimuthal variations of the microwave radiation from a slightly non-Gaussian sea surface. *Radio Sci*. **2000**, *35*, 65-82.
7. Trokhimovski, Y. G.; Irisov, V. G.; Westwater, E. R.; Fedor, L. S.; Leuski, V. E. Microwave polarimetric measurements of the sea surface brightness temperature from a blimp during the Coastal Ocean Probing Experiment (COPE). *J. Geophys. Res*. **2000**, *105*, 6501-6516.
8. Trokhimovski, Y.G.; Irisov, V. G. The analysis of wind exponents retrieved from microwave radar and radiometric measurements. *IEEE Trans. Geosci. Remote Sensing* **2000**, *38*, 470-479.
9. Yueh, S.H.; Kwok, R.; Li, F. K.; Nghiem, S. V.; Wilson, W. J.; Kong, J. A. Polarimetric passive remote sensing of ocean wind vectors. *Radio Sci.* **1994**, *29*, 799-814.
10. Reul, N.; Chapron, B. A simple algorithm for sea surface salinity retrieval from L-band radiometric measurements at nadir, *Proc. Int. Geoscience and Remote Sensing Symp. (IGARSS)* **2003**, Toulouse, France, IEEE, vol. 4, 2783-2785.
11. Tran, N.; Vandemark, D.; Ruf, C. S.; Chapron, B. The dependence of nadir ocean surface emissivity on wind vector with microwave radiometer, *IEEE Trans. Geosci. Remote Sensing* **2002**, *40*, 515-523.
12. Elfouhaily, T.M.; Guérin, C.-A. A critical survey of approximate scattering wave theories from random rough surfaces. *Waves Random Media* **2004**, 14, R1-R40.
13. Chapron, B.; Katsaros, K.; Elfouhaily, T.; Vandemark, D. A note on relationships between sea surface roughness and altimeter backscatter, *Air-Water Gas Transfer*, B. Jähne and E.C. Monahan, Eds., AEON Verlag & Studio, 869-878, **1995**.
14. Elfouhaily, T.; Vandemark, D.; Gourrion, J.; Chapron, B. Estimation of wind stress using dual-frequency TOPEX data. *J. Geophys. Res*. **1998**, *103*, 25101-25108.
15. Gourrion, J.; Vandemark, D.; Bailey, S.; Chapron, B.; Gommenginger, C. P.; Challenor, P. G.; Srokosz, M. A. A two-parameter wind speed algorithm for Ku-band altimeters. *J. Atmos. Oceanic Technol*. **2002**, *19*, 2030-2048.
16. Tran, N.; Zanife, O.-Z.; Chapron, B.; Vandemark, D.; Vincent, P. Absolute calibration of Jason-1 and Envisat altimeter Ku-band radar cross-section from cross-comparison with TRMM precipitation radar measurements. *J. Atmos. Oceanic Technol.* **2005**, *22*, 1389-1402.
17. Carayon, G.; Steunou, N.; Courriere, J.-L.; Thibaut, P. Poseidon-2 radar altimeter design and results of in-flight performances. *Mar. Geod.* **2003**, *26*, 156-165.
18. Marth, P.C.; Jensen, J. R.; Kilgus, C. C.; Perschy, J. A.; MacArthur, J. L.; Hancock, D. W.; Hayne, G. S.; Purdy, C. L.; Rossi, L. C.; Koblinsky, C. J. Prelaunch performance of the NASA altimeter for the TOPEX/Poseidon project. *IEEE Trans. Geosci. Remote Sens.* **1993**, *31*, 315-332.
19. Quilfen, Y.; Chapron, B.; Bentamy, A.; Gourrion, J.; Elfouhaily, T.; Vandemark, D. Global ERS-1/-2 and NSCAT observations - Upwind/crosswind and upwind/downwind measurements. *J. Geophys. Res*. **1999**, *104*, 11459-11469.
20. Kudryavtsev, V.; Johannessen, J. On effect of wave breaking on short wind waves. *Geophys. Res. Lett.* **2004**, 31, L20310, doi:10.1029/2004GL020619.

21. Karaev, V.Yu.; Kanevsky, M. B.; Cotton, P. D.; Challenor, P. G. Is it possible to measure ocean surface slopes with a microwave radar at nadir probing? *Int. J. Remote Sensing* **2002**, *23*, 3251-3262.
22. Elfouhaily, T.; Guignard, S.; Thompson, D. R. A practical second-order electromagnetic model in the quasi-specular regime based on the curvature of a 'good-conducting' scattering surface. *Waves in Random Media* **2003**, *13*, L1-L6.
23. Gardachov, R.G. The probability density of the total curvature of a uniform random Gaussian sea surface in the specular points. *Int. J. Remote Sensing* **2000**, *21*, 2917-2926.
24. Reul, N.; Branger, H.; Giovanangeli, J.-P.; Bliven, L. F. The influence of oblique waves on the azimuthal response of a Ku-band scatterometer - A laboratory study. *IEEE Trans. Geosci. Remote Sensing* **1999**, *37*, 36-47.